A cryogenically cooled, ultra-high-energy-resolution, trap-based positron beam

M. R. Natisin,[a] J. R. Danielson, and C. M. Surko
Department of Physics, University of California, San Diego, La Jolla, California 92093, USA

(Received 3 December 2015; accepted 31 December 2015; published online 12 January 2016)

A technique is described to produce a pulsed, magnetically guided positron beam with significantly improved beam characteristics over those available previously. A pulsed, room-temperature positron beam from a buffer gas trap is used as input to a trap that captures the positrons, compresses them both radially and axially, and cools them to 50 K on a cryogenic CO buffer gas before ejecting them as a pulsed beam. The *total* energy spread of the beam formed using this technique is 6.9 ± 0.7 meV FWHM, which is a factor of $\sim$5 better than the previous state-of-the-art, while simultaneously having sub-microsecond temporal resolution and millimeter spatial resolution. Possible further improvements in beam quality are discussed. © *2016 AIP Publishing LLC*.
[http://dx.doi.org/10.1063/1.4939854]

The buffer gas trap (BGT) has become the standard method of producing pulsed, high-energy-resolution positron beams for a variety of applications including the study of atomic and molecular scattering,[1] annihilation processes,[2] material science,[3] antihydrogen,[4–7] and positronium formation.[8] The BGT technique is used to produce high resolution beams by trapping and cooling positrons through interactions with room temperature molecular gases and subsequently ejecting them as pulsed beams ranging from ~ 0.1 eV to kilovolt energies. The state-of-the-art positron beam with regard to energy resolution in the literature was produced by our BGT and had a total energy spread $\Delta E_t = 34$ meV full width at half maximum (FWHM), along with a temporal spread $\Delta\tau = 1.7\,\mu$s and beam diameter $\Delta R = 1.0$ cm at 65 mT (cf. Figs. 3–5 of Ref. 9; radial distribution not shown). While this resolution is sufficient to probe well-isolated features at relatively low energies, many important interactions are difficult or impossible to study without further advances in beam technology.

The processes of positron cooling and beam formation in the BGT have recently been studied in detail.[9–11] Under typical conditions, beam formation is intrinsically dynamical. In particular, the particle dynamics just before ejection are crucial in setting beam quality. It was also shown that cooling the positrons to low temperatures prior to ejection should yield significantly improved energy and temporal resolution, and that trap geometries which create narrow, parabolic trapping potentials result in optimal beam quality. Using these results, a trap-based beam system was built with the goal of achieving significantly improved energy resolution together with improved spatial and temporal resolution.

The apparatus, called the cryogenic beam-tailoring trap (CBT), is placed after the BGT where it re-traps the incident, room-temperature positrons, compresses them both radially and axially, and further cools them through interactions with a cryogenically cooled buffer gas before ejecting them as a pulsed beam. Using this technique, positrons have been cooled to temperatures as low as 50 K, and beam pulses of $\sim 10^4$ positrons with total energy spreads as low as 6.9 meV FWHM have been produced. This is a factor of 5 better than the previous state-of-the-art. Further, due to the axial and radial compression, these beams also have sub-microsecond temporal spreads and beam diameters as small as 1 mm at 65 mT, corresponding to improvements over the state-of-the-art BGT beam by factors of $\sim$2 and $\sim$10, respectively.

The operation of the BGT-based beam, used as input to the CBT, has been described in detail elsewhere.[2] High energy positrons are emitted from a ^{22}Na radioactive source and slowed to electron-volt energies using a layer of solid Ne maintained at $\sim$8 K.[12] This steady-state beam is magnetically guided into a three stage BGT, which consists of a modified Penning-Malmberg trap in a $\sim$0.1 T magnetic field, where the positrons are trapped and cooled through rotational excitation of a 300 K N_2 buffer gas. Note that, in the previous work, a CF_4 buffer gas was used in addition to the N_2 for more rapid cooling by vibrational excitation of the CF_4; however, this step is omitted here to prevent freezing of the CF_4 on the adjacent CBT electrodes. Additionally, since the BGT beam is further processed in the CBT, it was not necessary to fully cool the positrons to 300 K in the BGT. After the positrons have been cooled for $\sim$0.1 s, the potential well is rapidly increased, lifting the particles over a potential barrier and ejecting them as a pulsed beam with a typical parallel energy spread of $\Delta E_{\parallel} \sim 100$ meV FWHM and a temporal spread of $\Delta\tau \sim 1\,\mu$s FWHM. This beam is then used as input to the CBT.

As seen in Fig. 1, the CBT consists of eight cylindrically symmetric electrodes surrounded by a cylindrical shell. The electrodes are made of oxygen-free high purity copper (OFHC) and were originally plated with a silver diffusion barrier followed by a gold overlayer. However, for improved electrode performance, the inner diameter surfaces of the electrodes were subsequently coated with a colloidal graphite solution (Aquadag), as discussed below. The upstream face of the electrode package is attached through a cold finger to a cryo-cooler maintained at $\sim$12 K, yielding electrode temperatures of $\sim$46 K and $\sim$54 K as measured at the

[a]Author to whom correspondence should be addressed. Electronic mail: mnatisin@physics.ucsd.edu

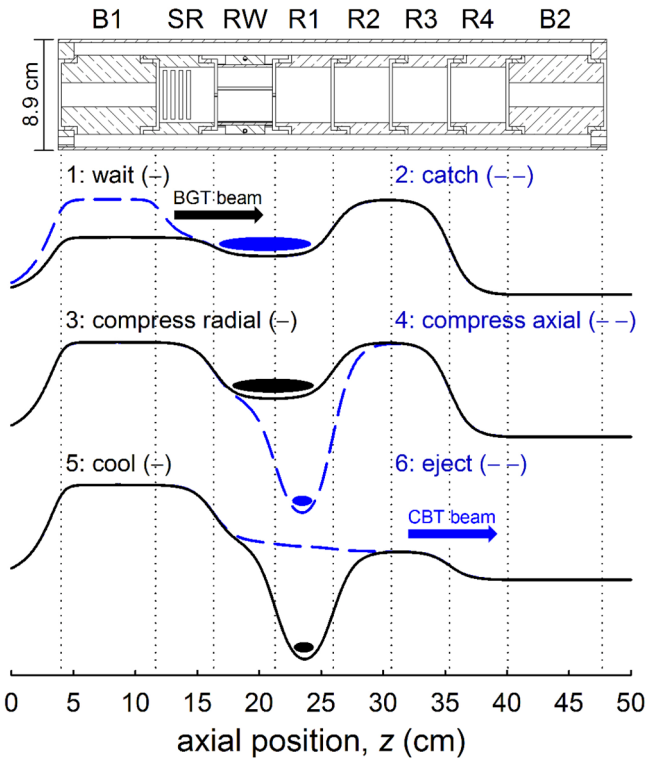

FIG. 1. Schematic of the CBT electrodes and potentials during each of its six phases. Electrodes from left to right are the baffle B1, slotted ring SR, rotating wall RW, cylindrical rings R1-R4, and baffle B2. Phases are labeled according to the order in which they proceed, (—) shows phases 1, 3, and 5 and (– – ––) shows phases 2, 4, and 6. Shaded regions and arrows represent the positrons in various phases.

outermost electrodes B1 and B2 in Fig. 1. Room-temperature buffer gas, typically CO, is injected into the region between the inside of the outer shell and the outside of the electrodes, where it cools to the ~50 K electrode temperature through collisions with the cold surfaces. The now ~50 K buffer gas makes its way through the slots in electrode SR into the inner cavity, where it has an estimated typical pressure of ~1 μTorr and is able to interact with the trapped positrons.

The CBT operates in six phases, as shown in Fig. 1. Initially, the potentials are set to catch the incident BGT pulse, during which time the BGT fill, cool, and eject phases are completed. Approximately 10 μs after the BGT eject phase is triggered, the incident pulse is "caught" by gate-switching electrode B1. The re-trapped positrons are compressed radially for ~0.2 s using the so-called "single-particle regime rotating wall" technique of applying an azimuthally rotating electric field to the 4-segmented electrode labeled RW.[13–15] The positrons are then axially compressed by applying a negative voltage to R1, thus pulling them into a narrow parabolic potential well, in order to induce a strong magnetron motion for better radial confinement during cooling and to increase the amount of adiabatic cooling during ejection.[9,11] At this point, the positrons are cooled through interactions with the ~50 K CO buffer gas for ~0.2 s and subsequently ejected by increasing the R1 voltage, lifting them over the potential barrier generated by R2 and R3 and ejecting them as a pulsed, cryogenic positron beam.

Under typical conditions, the total shot-to-shot time (including BGT phases) is ~0.8 s for ~10^4 positrons per pulse from the CBT, with a re-trapping efficiency (i.e., BGT to CBT) of ~60%. This represents a 40% loss which appears to be primarily due to the fact that the incident BGT beam diameter is comparable to the inner diameter of the CBT baffle electrodes (baffle ID = 1.9 cm, cf. inset of Fig. 3(b) for BGT beam *radial* profile), and the fact that there is significant asymmetry-induced radial expansion of the positrons before they are compressed by the rotating wall.

When trapping in an approximately parabolic potential in the region beyond the SR and RW electrodes (i.e., the electrodes with azimuthal asymmetries), ~100% re-trapping has been obtained, and this is in agreement with simulations. However, the re-trapping efficiency is reduced when using non-parabolic trapping potentials or trapping in a region which includes the SR or RW electrodes, both of which are required for operation of the rotating wall. The buffer gas and pressure also affect the efficiency, but to a lesser extent. These results indicate that radial compression of the incident BGT beam would likely result in a near-unity re-trapping efficiency.

Using this technique, positrons have been cooled to 50 K with either a CO or N_2 buffer gas. In the case of CO, the positrons are cooled primarily through vibrational excitation of the CO stretch mode at high temperatures, then rotational excitation at low temperatures by coupling to both the CO dipole and quadrupole moments.[10] In the case of N_2, positron cooling is significantly slower due to quadrupole-coupled rotational excitation being the dominant cooling channel. It should be noted that while positrons were cooled to 50 K using either a CO or N_2 buffer gas, radial compression was only significant when using CO. When using an N_2 buffer gas, no appreciable radial compression was achieved. For this reason, and due to CO yielding significantly faster cooling rates, the beam results discussed here were all obtained using a CO buffer gas.

The resulting parallel, perpendicular, and total energy distributions obtained from the CBT are shown in Fig. 2. The methods used to obtain these distributions have been described in detail elsewhere.[9] The parallel energy distribution is well fit by a Gaussian with $\Delta E_{\parallel} = 4.0 \pm 0.2$ meV FWHM and a standard deviation $\sigma_{\parallel} = 1.7 \pm 0.1$ meV. The perpendicular energy distribution is a Maxwell-Boltzmann with $\sigma_{\perp} = 4.5 \pm 0.3$ meV, corresponding to a positron temperature of 52.4 ± 3.7 K. Finally, the total energy distribution is a convolution of the parallel and perpendicular components, resulting in an exponentially modified Gaussian (EMG) distribution with an energy resolution $\Delta E_t = 6.9 \pm 0.7$ meV ($\sigma_t = 4.8 \pm 0.3$ meV). This is a factor of ~5 better than that obtained by the previous state-of-the-art positron beam, as shown in the inset of Fig. 2(c).[9]

Several difficulties were encountered in producing and measuring parallel energy spreads of the order of a few milli-electron volts. A key impediment is due to potential variations on the electrode surfaces (i.e., on the CBT electrodes and on the retarding potential analyzer (RPA) electrode used to measure the beam distribution), which result in a broadening of the measured parallel energy distribution.[16–18] These so-called "patch potentials" appear to be accentuated by buffer gas molecules sticking on the cold CBT electrodes. As noted above, the CBT was installed with gold-plated

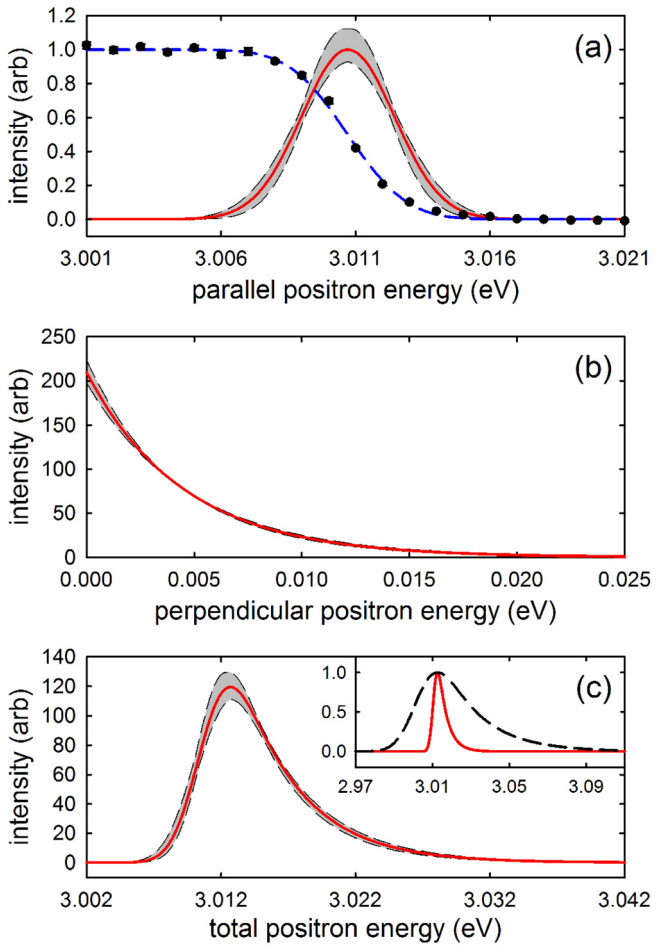

FIG. 2. (—) Beam energy distributions from the CBT: (a) (•) measured cumulative parallel energy distribution, (– – ––) Gaussian fit to data yielding $\Delta E_{\|} = 4.0 \pm 0.2$ meV FWHM, (b) Maxwell-Boltzmann perpendicular energy distribution corresponding to a measured mean perpendicular energy of 4.5 ± 0.3 meV (52.4 ± 3.7 K), and (c) convolution of curves in (a) and (b), yielding $\Delta E_t = 6.9 \pm 0.7$ meV FWHM. Shaded regions show 95% confidence intervals estimated from the fits. The inset in (c) shows the total energy distribution obtained from (—) CBT and (– – ––) state-of-the-art BGT (cf. Fig. 5(c) of Ref. 9).

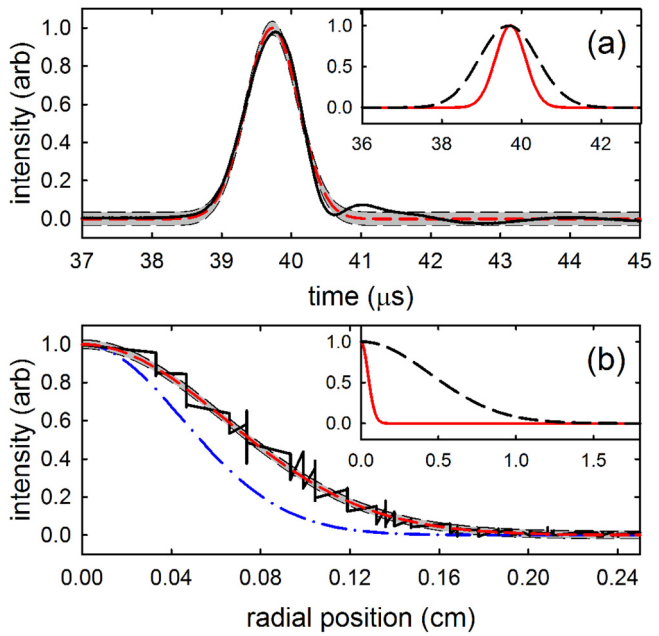

FIG. 3. (—) (a) Temporal and (b) radial beam distributions from the CBT as measured at the phosphor screen (32 mT). (– – ––) Gaussian fits to data yielding $\Delta\tau = 0.88 \pm 0.01\ \mu$ s FWHM and $\Delta R = 0.15 \pm 0.001$ cm FWHM, respectively. (– · –) Estimated radial distribution in CBT (65 mT) with $\Delta R \approx 0.1$ cm FWHM. Shaded regions show the 95% confidence intervals estimated from fits. Insets show fits to (a) temporal distribution obtained from (—) CBT and (– – ––) state-of-the-art BGT (cf. Fig. 3 of Ref. 9), and (b) radial distribution at 65 mT obtained from (—) CBT and (– – ––) state-of-the-art BGT.

copper electrodes, for which the parallel energy spreads were limited to $\gtrsim 10$ meV FWHM. The inner surfaces of the trap electrodes and RPA were subsequently coated with a colloidal graphite solution, and this significantly improved the energy resolution, particle confinement times, and shot-to-shot reproducibility.

While the primary goal of the CBT was to provide significantly improved energy resolution over existing techniques, other characteristics of the resulting beam were also improved. Shown in Fig. 3 are the measured temporal and radial distributions, obtained under the same conditions as those shown in Fig. 2, with the insets comparing these results to those obtained for the previous state-of-the-art energy resolution beam.[9] The temporal distribution was measured by impinging the beam against a metal plate and measuring the gamma-ray signal produced by the annihilations. The temporal distribution is approximately Gaussian with $\Delta\tau = 0.88 \pm 0.01\ \mu$s FWHM, corresponding to a factor of ~ 2 improvement over the previous state-of-the-art energy resolution beam. It should be noted that the response time of the detector and associated electronics was $\sim 0.5\ \mu$s FWHM, thus representing a non-negligible contribution to the measured temporal distribution, and therefore this measurement represents an upper bound. Under different conditions (e.g., increasing the positron ejection rate), significantly narrower temporal spreads may be obtained at the cost of energy resolution. However, due to the limitations of the current detection apparatus, the ultimate limit of the temporal resolution has not yet been measured.

The radial distribution, shown in Fig. 3(b), is measured by accelerating the beam to -10 kV and allowing it to impinge on a phosphor screen. The resulting light is recorded with a CCD camera and the data averaged azimuthally. The measured radial distribution is fit to a Gaussian, yielding a beam diameter of $\Delta R = 0.15 \pm 0.001$ cm FWHM at the phosphor screen. Taking into consideration the fact that the screen is in a lower magnetic field than the CBT (approximately 32 mT *vs.* 65 mT, respectively), the measurements indicate that the beam diameter in the CBT is approximately 1 mm. This is a full order of magnitude improvement over the BGT beam. For reference, without the radial compression using the RW, the beam diameter in the CBT is approximately 1 cm FWHM.

The significantly narrower total energy distribution obtained from the CBT has several practical advantages. This narrower energy spread allows approximately five times more densely packed energy-spectral features to be resolved in comparison with previous capabilities. This is, for example, particularly useful for studying annihilation processes such as intramolecular vibrational redistribution (IVR).[19] It is also expected to be sufficient to enable the direct measurements of positron-induced multimode excitations.[20] Additionally, it is sufficient to permit measurements of features down to

approximately five times lower energy, potentially enabling state-resolved measurements of rotational excitation by positron impact. Finally, the narrower total energy distribution yields approximately five times better signal-to-noise ratios as compared to those obtained previously.

Computer simulations[9,11] indicate that the present CBT apparatus operating at 50 K should ideally be able to obtain parallel energy spreads which are a factor of 4 lower than the currently measured value of 4.0 meV FWHM. While not completely certain, this discrepancy could be due to remaining effects of the patch potentials discussed above. Work to mitigate these extraneous effects continues. Additionally, the beam could be further improved if the CBT were operated at an even lower temperature. Using CO or N_2, it should be possible to operate with buffer gas temperatures as low as ~30 K, where simulations predict total energy spreads as low as 2.5 meV FWHM could be obtained.

In summary, the CBT uses the now standard BGT-based room temperature beam as input, compresses the beam both radially and axially, and further cools the positrons before ejecting them as a pulsed beam with superior characteristics. Using this technique, positrons have been cooled to 50 K through interactions with CO or N_2 buffer gases, and positron beams have been produced which have a 6.9 meV total energy resolution, sub-microsecond temporal resolution, and millimeter spatial resolution. As discussed above, further improvements in beam quality appear to be possible using the approach described here.

We wish to thank E. A. Jerzewski for expert technical assistance and S. Robertson for helpful discussions regarding the use of the Aquadag coating. This work was supported by the NSF (Grant No. PHY 14-01794).

[1]C. M. Surko, G. F. Gribakin, and S. J. Buckman, J. Phys. B: At. Mol. Opt. Phys. **38**, R57 (2005).
[2]G. F. Gribakin, J. A. Young, and C. M. Surko, Rev. Mod. Phys. **82**, 2557 (2010).
[3]D. Chaudhary, M. Went, K. Nakagawa, S. Buckman, and J. Sullivan, Mater. Lett. **64**, 2635 (2010).
[4]M. Amoretti, C. Amsler, G. Bonomi, A. Bouchta, P. Bowe, C. Carraro, C. L. Cesar, M. Charlton, M. J. T. Collier, M. Doser, V. Filippini, K. S. Fine, A. Fontana, M. C. Fujiwara, R. Funakoshi, P. Genova, J. S. Hangst, R. S. Hayano, M. H. Holzscheiter, L. V. Jorgensen, V. Lagomarsino, R. Landua, D. Lindelof, E. L. Rizzini, M. Macri, N. Madsen, G. Manuzio, M. Marchesotti, P. Montagna, H. Pruys, C. Regenfus, P. Riedler, J. Rochet, A. Rotondi, G. Rouleau, G. Testera, A. Variola, T. L. Watson, and D. P. van der Werf, Nature **419**, 456 (2002).
[5]G. Gabrielse, N. S. Bowden, P. Oxley, A. Speck, C. H. Storry, J. N. Tan, M. Wessels, D. Grzonka, W. Oelert, G. Schepers, T. Sefzick, J. Walz, H. Pittner, T. W. Hänsch, and E. A. Hessels (ATRAP Collaboration), Phys. Rev. Lett. **89**, 213401 (2002).
[6]G. B. Andresen, M. D. Ashkezari, M. Baquero-Ruiz, W. Bertsche, P. D. Bowe, E. Butler, C. L. Cesar, S. Chapman, M. Charlton, A. Deller, S. Eriksson, J. Fajans, T. Friesen, M. C. Fujiwara, D. R. Gill, A. Gutierrez, J. S. Hangst, W. N. Hardy, M. E. Hayden, A. J. Humphries, R. Hydomako, M. J. Jenkins, S. Jonsell, L. V. Jorgensen, L. Kurchaninov, N. Madsen, S. Menary, P. Nolan, K. Olchanski, A. Olin, A. Povilus, P. Pusa, F. Robicheaux, E. Sarid, S. S. e. Nasr, D. M. Silveira, C. So, J. W. Storey, R. I. Thompson, D. P. van der Werf, J. S. Wurtele, and Y. Yamazaki, Nature **468**, 673 (2010).
[7]G. Gabrielse, R. Kalra, W. S. Kolthammer, R. McConnell, P. Richerme, D. Grzonka, W. Oelert, T. Sefzick, M. Zielinski, D. W. Fitzakerley, M. C. George, E. A. Hessels, C. H. Storry, M. Weel, A. Müllers, and J. Walz (ATRAP Collaboration), Phys. Rev. Lett. **108**, 113002 (2012).
[8]D. B. Cassidy and A. P. Mills, Nature **449**, 195 (2007).
[9]M. R. Natisin, J. R. Danielson, and C. M. Surko, Phys. Plasmas **22**, 033501 (2015).
[10]M. R. Natisin, J. R. Danielson, and C. M. Surko, J. Phys. B **47**, 225209 (2014).
[11]M. R. Natisin, J. R. Danielson, and C. M. Surko, "Formation Mechanisms and Optimization of Trap-Based Positron Beams," Phys. Plasmas (submitted).
[12]R. G. Greaves and C. M. Surko, Can. J. Phys. **74**, 445 (1996).
[13]R. G. Greaves and C. M. Surko, Phys. Rev. Lett. **85**, 1883 (2000).
[14]R. G. Greaves and J. M. Moxom, Phys. Plasmas **15**, 072304 (2008).
[15]C. A. Isaac, C. J. Baker, T. Mortensen, D. P. van der Werf, and M. Charlton, Phys. Rev. Lett. **107**, 033201 (2011).
[16]T. W. Darling, F. Rossi, G. I. Opat, and G. F. Moorhead, Rev. Mod. Phys. **64**, 237 (1992).
[17]J. B. Camp, T. W. Darling, and R. E. Brown, J. Appl. Phys. **69**, 7126 (1991).
[18]S. Robertson, Z. Sternovsky, and B. Walch, Phys. Plasmas **11**, 1753 (2004).
[19]A. C. L. Jones, J. R. Danielson, M. R. Natisin, and C. M. Surko, Phys. Rev. Lett. **110**, 223201 (2013).
[20]A. C. L. Jones, J. R. Danielson, M. R. Natisin, C. M. Surko, and G. F. Gribakin, Phys. Rev. Lett. **108**, 093201 (2012).